



HAL
open science

Visual-based Global Localization from Ceiling Images using Convolutional Neural Networks

Philip Scales, Mykhailo Rimel, Olivier Aycard

► **To cite this version:**

Philip Scales, Mykhailo Rimel, Olivier Aycard. Visual-based Global Localization from Ceiling Images using Convolutional Neural Networks. 16th International Conference on Computer Vision Theory and Applications, Feb 2021, Online Streaming, France. pp.927-934, 10.5220/0010248409270934 . hal-03196336

HAL Id: hal-03196336

<https://hal.univ-grenoble-alpes.fr/hal-03196336>

Submitted on 12 Apr 2021

HAL is a multi-disciplinary open access archive for the deposit and dissemination of scientific research documents, whether they are published or not. The documents may come from teaching and research institutions in France or abroad, or from public or private research centers.

L'archive ouverte pluridisciplinaire **HAL**, est destinée au dépôt et à la diffusion de documents scientifiques de niveau recherche, publiés ou non, émanant des établissements d'enseignement et de recherche français ou étrangers, des laboratoires publics ou privés.

Visual-based Global Localization from Ceiling Images Using Convolutional Neural Networks

Philip Scales¹, Mykhailo Rimel², Olivier Aycard¹

¹LIG-MARVIN, Université Grenoble Alpes, 621 Avenue Centrale, Saint-Martin-d'Hères, France

²Department of Computer science, Grenoble INP, 46 Avenue Félix Viallet, Grenoble, France
{philip.scales, aycardol}@univ-grenoble-alpes.fr, mykhailo.rimel@grenoble-inp.org

Keywords: Visual-based Localization, CNN, Mobile Robot

Abstract: The problem of global localization consists in determining the position of a mobile robot inside its environment without any prior knowledge of its position. Existing approaches for indoor localization present drawbacks such as the need to prepare the environment, dependency on specific features of the environment, and high quality sensor and computing hardware requirements. We focus on ceiling-based localization that is usable in crowded areas and does not require expensive hardware. While the global goal of our research is to develop a complete robust global indoor localization framework for a wheeled mobile robot, in this paper we focus on one part of this framework – being able to determine a robot’s pose (2-DoF position plus orientation) from a single ceiling image. We use convolutional neural networks to learn the correspondence between a single image of the ceiling of the room, and the mobile robot’s pose. We conduct experiments in real-world indoor environments that are significantly larger than those used in state of the art learning-based 6-DoF pose estimation methods. In spite of the difference in environment size, our method yields comparable accuracy.

1 INTRODUCTION

Localization is essential for any autonomous or semi-autonomous mobile robot. A robot must know its pose relative to the environment in order to be able to make decisions, move or perform actions. In a broad sense, the goal of localization is to provide the robot's pose. Depending on the context, it can be a pose in the world, in a specific environment or with respect to some other object. In the case of global localization, the robot must determine its pose without any prior assumptions, enabling it to solve the Kidnapping problem. With the increasing interest in social robotics, we are seeing robots deployed in hospitals, shopping malls, care homes, and other human-populated indoor environments. We consider the problem of globally localizing the robot within crowded indoor environments.

Different sensors can be used to estimate motion and/or acquire observations, the most frequently used being laser range finders (LRFs) and cameras. However, all sensors have their limitations, usually making them applicable only in certain conditions and/or environments. When using LRFs in crowded environments, a large proportion of laser hits will provide distances to people which is not relevant for localization. Furthermore, laser range finders are

orders of magnitude more expensive than cameras. There are also a number of solutions requiring some modification of the environment, such as setting up wireless beacons, or installing artificial landmarks and visual features. We aim to avoid modifying the environment, since this may not be possible, or may be too costly in some real-world applications. When solving a localization problem, the map of the environment may or may not be given as input. If the map is not given, the problem is Simultaneous Localization and Mapping (SLAM) (Bailey and Durrant-Whyte, 2006), which we will not consider.

We aim to develop a real-time framework for the indoor global localization of a wheeled mobile robot, which can be applied in crowded environments with varying lighting conditions. As a first step towards a complete framework, in this paper, we provide a method for estimating the robot’s pose from a single ceiling image. This method can be used with mid-range, relatively low-cost hardware. Additionally, our method is straightforward to implement, and all its dependencies are open-source software. We propose to use a supervised learning approach — Convolutional Neural Networks (CNNs) — to estimate the robot’s 2-DoF position and orientation angle from a single ceiling image taken by a fisheye camera mounted on the robot.

2 RELATED WORK

Taking into account the assumptions we have made in the Introduction, in this section we focus on the review of vision-based methods for mobile robot localization. These methods can vary depending on where the camera is mounted, how features are extracted from the acquired images, and in which environment the robot is intended to operate.

Some works (Jin and Lee, 2004; Delibasis et al., 2015) use ceiling-mounted cameras to perform the localization of an indoor mobile robot. The former uses neural networks to detect a robot in an image and the latter uses segmentation techniques with a robot marked with a specific color. Front-facing cameras were used in (Kendall et al., 2015; Kendall et al., 2017; Clark et al., 2017; Brahmbatt et al., 2018; Kendall et al., 2016) to perform indoor and outdoor 6-DoF camera relocalization. Although their task was not to localize a mobile robot, their findings are relevant to our problem. There are also approaches for general place recognition (Zhang et al., 2016) which do not provide sufficient accuracy for robot localization. CNNs are useful in image classification tasks since they are able to extract features from images (Krizhevsky et al., 2012). The CNN presented in (Kendall et al., 2015) is able to recognize high-level features, such as building contours, and learns the relation between those features and the pose of the camera. This allows them to regress the 6-DoF pose from an RGB image in real-time.

An alternative is to mount an upwards-facing camera on top of the robot. We will refer to these as ceiling-vision cameras, the first use of which was in (King and Weiman, 1991). The earlier publications relied on the presence of active lights on the ceiling to perform localization, with (Thrun et al., 1999) measuring the brightness of a local patch of the ceiling above the robot. More approaches have been developed since then including the use of artificial markers (e.g. barcodes, April tags, infra-red beacons etc.) (Nourbakhsh, 1998) and extracting primitives (e.g. lines, corners etc.) (Jeong and Lee, 2005). In (Thrun, 1998), ceiling-vision cameras and artificial neural networks were used to recognize manually defined high-level features. However, they used individual networks for each feature, and their experiments were limited to a corridor environment.

Approaches using a front-facing camera may fail in situations where many dynamic obstacles obstruct recognizable features of the environment. Our use of a ceiling-vision camera aims to limit such obstructions. Approaches using ceiling-mounted cameras or artificial landmarks require the environment to be modified, and the use of ceiling lights is only feasible in environments where the

lights are constantly switched on. The use of manually-defined high-level features makes it harder to adopt the algorithm for various types of ceilings composed of different types of panels or lamps.

There are a few fundamental differences between the applications of our approach and the applications considered for camera relocalization (Kendall et al., 2015; Kendall et al., 2017; Clark et al., 2017; Brahmbatt et al., 2018; Kendall et al., 2016). These works obtained high 6-DoF pose accuracy (0.18-0.48m, 0.11-0.17rad) using the 7-Scenes dataset (Zhang et al., 2016) which was acquired in small indoor environments (2-12m², 1-1.5m height). They also evaluate their methods in larger outdoor environments (875-50000m²), but the accuracy obtained is insufficient for indoor localization of a mobile robot (1.46-3.67m, 0.13-0.25rad). In contrast, we aim to provide accurate localization at any point of rooms of around 100m². Furthermore, images of ceilings generally contain less visual features than images from either outdoor or 7-scenes datasets. Finally, these works do not evaluate the performance of their networks on more constrained embedded hardware typical for indoor mobile robots.

A more recent work (Xiao et al. 2019) explores how to ignore dynamic objects when performing visual SLAM using deep CNNs.

3 METHODS

3.1 Overview

In this paper, we combine the use of a ceiling-vision camera and CNNs to estimate the pose of a mobile robot. Our ceiling-image localization module takes a single raw camera image as input, and outputs the position $[x,y]$ and orientation θ of the robot in the frame of an existing map of the environment. We motivate our choices in section 3.2.

The localization module we propose operates in two steps. In step one, an image of the ceiling is acquired using a camera mounted on top of a wheeled robot. The raw camera image undergoes pre-processing which is described in section 3.3. In step two, the pre-processed image is used as the input to two CNNs, which were separately trained to predict robot position and orientation from a ceiling image. Position and orientation predictions are combined to form the 3-DoF pose prediction which is directly used for robot localization. In the scope of this work, we do not consider applying additional filters or sensor fusion. The CNN architectures are described in section 3.4. Details of dataset construction are given in section 3.5. The steps for localizing the robot are

summarized in Fig. 1. Pseudo-code for the pose update is provided in Fig. 2.

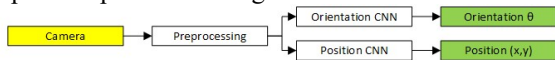


Figure 1: Summary of the localization module.

3.2 Motivation

CNNs learn which features are relevant to a given dataset and task, so applying our method to a new environment requires only a new dataset and network training, as opposed to manual tweaking of pre-defined features. Inspired by works in the field of place recognition and 6-DOF camera relocalization, we use CNNs to estimate the 3-DoF pose of the robot from an image. CNNs for complex tasks have a high memory and computational cost. We split the task into the estimation of the 2-DoF position, and estimation of the orientation, each of which is treated as a regression problem solved by a separate CNN. This was more accurate than using a single CNN with our architecture to regress the full 3-DoF pose.

Using only a ceiling image as input allows our approach to provide immediate global localization, without the need for an external initial pose estimation as input or environment exploration phase.

```

Input: cameraImage img
Output: pose p
Algorithm:
img ← receive_image()
img ← resize(img, 160, 120)
img ← convert_to_greyscale(img)
img ← apply_clahe(img)
p.position ←
  position_cnn.predict(img)
p.orientation ←
  orientation_cnn.predict(img)
publish_pose(p)
  
```

Figure 2: Pseudocode of one localization cycle.

3.3 Image Pre-processing

The input images to the CNN are obtained by applying a pre-processing step to the camera images; they are resized to a resolution of 160x120 pixels, converted to greyscale, and contrast-limited adaptive histogram equalization (CLAHE) (Pizer et al., 1987) is applied to them. The image resolution was chosen as a trade-off between the localization accuracy, and the size and computational requirements of the CNN. We decided to disregard the color information because there are few color features on most ceilings. CLAHE was applied to make the network less sensitive to changes in ambient lighting.

3.4 CNN Architectures

In order to design our CNN, we experimented with various network architectures. We decided to use the same base CNN architecture to construct our position and orientation CNNs, with the only difference being the number of outputs. We base our final architecture on only a sub-part of the GoogLeNet architecture (Szegedy et al., 2015) because our task is different, and we target a lower computational cost.

Starting with the full GoogLeNet architecture, the process to build our CNN can be summarized as follows: (1) we took the first part of GoogLeNet (from Input to Softmax0 layer in Fig. 3 of (Szegedy et al., 2015)); (2) we adapted existing layers to suit our dataset and task by modifying the input layer to suit our images, and by adapting the output layer for regression; (3) we added Batch Normalization layers after the first two Maxpool layers; (4) we adjusted network hyperparameters. In the rest of this section, we detail our changes to the original GoogLeNet, with all unmentioned aspects left unchanged.

GoogLeNet can be understood as having two auxiliary classifiers branching off from the main classifier at earlier stages. Generally speaking, in CNNs, early layers close to the input learn filters that capture low-level features, and later layers closer to the output capture high-level features. Ceilings are usually made up of many lower-level features, such as lines, edges, lamps, exit signs, and ceiling panels. In contrast, GoogLeNet was designed to classify images into 1000 categories, each of which required the network to capture high-level features. This observation led us to make use of only the first auxiliary classifier, discarding other layers. The layer parameters such as number of units, number and size of filters, and their structure were left unchanged.

We adapted the input layer to our data by changing the input shape to 160x120x1 (width, height, channels) in order to suit our images, which are smaller than those used in GoogLeNet, and use only one color channel. Consequently, the sizes of our feature maps are different, and can be seen in Fig. 3. We adapted the output layer by replacing the softmax0 with a dense layer with one or two units for orientation or position regression respectively.

Batch normalization (Ioffe and Szegedy, 2015) consists in normalizing the inputs of a layer for each batch of images. This allows us to limit overfitting by improving regularization, which is especially needed when using small datasets such as ours. We introduced Batch normalization layers after each of the first two MaxPooling layers, as seen in Fig. 3.

Hyperparameters are tuned to maximize a network’s performance on a given task and dataset. We experimented with various parameters considering what worked best for our task, datasets,

and hardware. We replaced the stochastic gradient descent optimizer with the more recent Amsgrad (learning rate=0.001, beta1=0.9, beta2=0.999, epsilon=10⁻⁷, decay=0) (Reddi et al., 2018). We reduced the batch size for training from 256 to 16 to account for our dataset size, which is smaller than the one GoogLeNet was designed for. This also reduced the memory requirements when training the network, allowing us to target mid-range hardware. For the task of position estimation, we augmented the dataset by applying random rotations to the images. Given that our camera was centered on the robot, this was equivalent to capturing images from the same position at different orientations.

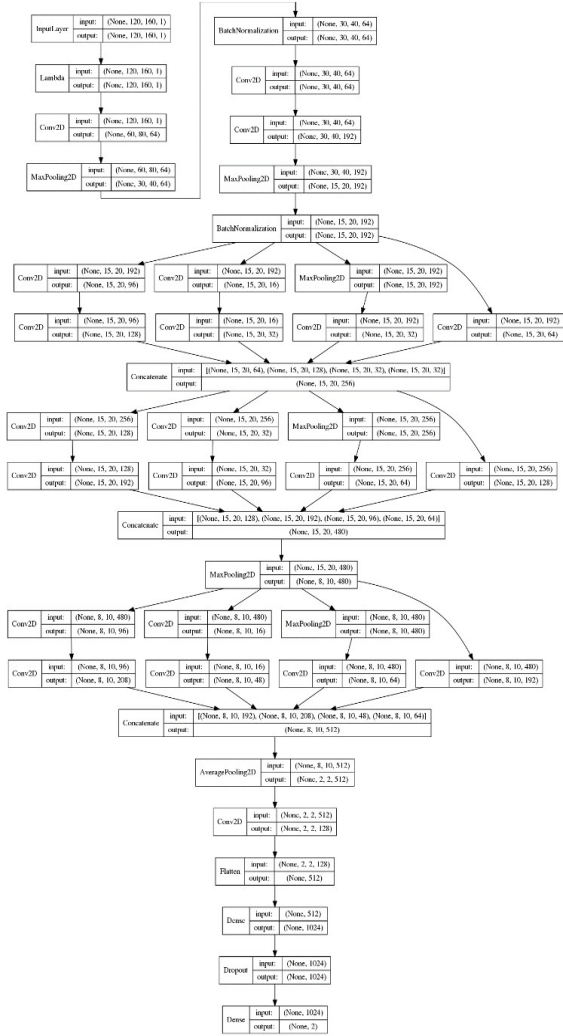


Figure 3: CNN for position regression with layer types and feature map shapes (*best viewed on the digital version*).

PoseNet (Kendall et al, 2015) and other similar works perform 6-DoF camera relocalization in town-scale outdoor, and room-scale indoor environments. These environments contain many high-level features

which are useful for camera relocalization. Since they deal with a less constrained problem and high-level features, they use larger networks. Our approach is a smaller architecture that still maintains sufficient representation capacity for our task.

3.5 Dataset Construction

The dataset required to train the CNNs is built by teleoperating the robot in the environment in which it will be deployed, while acquiring images of the ceiling along with the corresponding ground-truth poses. The images are pre-processed as described in section 3.3. The quality of the CNN’s predictions depends on the dataset, which is affected by the conditions in which the images are acquired, as well as the method by which the ground-truth pose is acquired. Artificial and natural lighting conditions were varied during data acquisition to improve the CNN’s robustness. For artificial lighting, data was acquired with all lights on, or all lights off. The ground-truth pose is provided by an alternative existing localization method. We used laser-based Adaptive Monte-Carlo Localization (AMCL) (Fox et al, 1999) coupled with an existing map of the environment to provide ground-truth measurements. We acquired data in a quasi-static environment in order to maximize the accuracy of the AMCL.

We discarded samples for which the ground-truth localization had reported a high uncertainty, which we defined as samples where any one of the pose covariances were higher than a threshold: $\sigma(x,x) > 0.15m^2$ or $\sigma(y,y) > 0.15m^2$ or $\sigma(\theta,\theta) > 0.1rad^2$. This does not eliminate the problem of the pose estimation drifting out of accuracy as the robot is teleoperated. To mitigate this effect, data acquisition was performed by combining data from several shorter acquisitions. Fig. 4 summarizes the data acquisition.

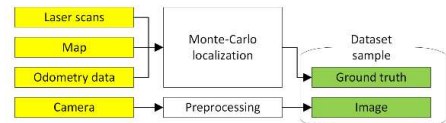


Figure 4: Overview of the data acquisition method.

4 EXPERIMENTAL SETUP AND RESULTS

We implemented our method in order to deploy it on RobAIR (“RobAIR”) (see Fig. 5), a wheeled mobile robot and tested it in real environments and situations. In this section, we describe the hardware, software, the experimental protocol, and results.

4.1 Environments and Datasets

We considered two environments (denoted as A and B - see Fig. 5) with different ceiling features. Their areas were 83 m² and 72 m², and ceiling heights of 4m and 2.5m for A and B respectively. A dataset was built for each environment by teleoperating the robot at a speed of 0.5 m/s. Images were acquired at 5fps and associated with their ground truth pose.

For environment A, 30105 samples were acquired (train, validation data split: 89.7%, 10.3%). For environment B, 27237 samples were acquired (train, validation split: 80.5%, 19.5%). For testing, we deployed the robot in three different scenarios: (1) an uncrowded environment; (2) an uncrowded environment with a new artificial lighting configuration; (3) an environment where several participants partially obstructed the camera’s view. In order to evaluate the performance of our approach, we teleoperated the robot while recording samples composed of the ceiling image, ground-truth pose, and our method’s pose prediction. New samples were taken when the ground-truth pose changed by more than 0.001m or 0.001rad in order to discard moments when the robot was stationary. We present statistics on position and orientation errors for the different scenarios in Table 1, computed using the testing datasets containing 400 to 600 samples, acquired over 320 to 609 seconds of operation.

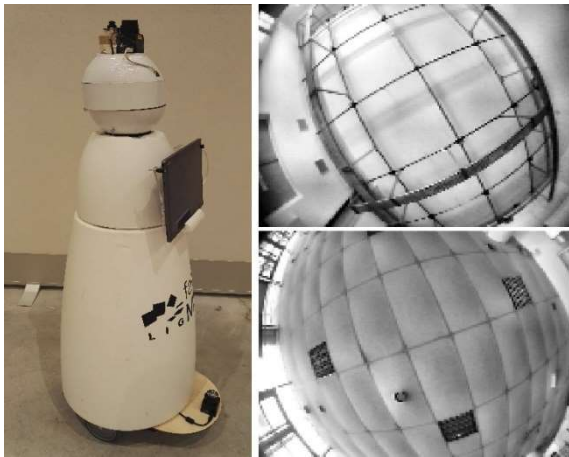


Figure 5: Left: RobAIR. Right: images of the ceiling in environments A (top) and B (bottom).

4.2 Implementation Details

The camera we used was a low-resolution (640x480 pixels) USB camera, equipped with a fish-eye lens. It was mounted on top of the RobAIR, at a height of 120cm. The robot was equipped with an i5-6200U processor. The full pose estimation step, from acquiring the image to outputting a pose took 100ms

to run on the robot’s processor. When performing localization, the camera recorded at 5fps, hence the pose update rate was 5Hz. We implemented the localization module as a ROS node. CNNs were implemented in Python using Keras with Tensorflow backend. Training was performed on a mid-range laptop GPU (Nvidia GTX 960m, 2GB of VRAM) using CUDA. Networks were trained for 30 epochs (about 1 hour each network). The laser for ground-truth pose acquisition was a Hokuyo URG-04LX-UG01 rangefinder, mounted on the base of RobAIR.

4.3 Experimental Results and Analysis

In Fig. 6 and Fig. 7, we show the histograms of pose error values for scenario 1, environment B. The supplementary video contains a visualization of the pose predictions in our evaluation scenarios, as well as the graphs of errors over the whole duration of each scenario, which give an idea of how the pose prediction behaves over time. For both position and orientation, the general trend in error values varies according to which part of the environment the robot is in. Error values fluctuate continuously during the evaluation, with occasional large error spikes. In all scenarios, the error behaves in a similar fashion.

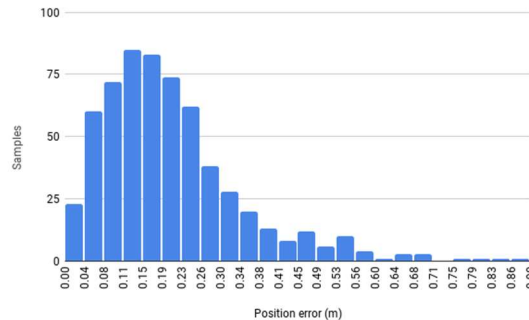


Figure 6: Position estimation error histogram for scenario 1 in environment B (609 samples).

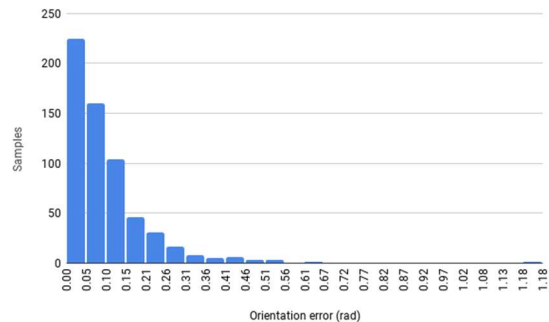


Figure 7: Orientation error histogram for scenario 1 in environment B (609 samples).

Scenario 1 consisted in sampling the data from the testing datasets used to evaluate the CNNs. These

datasets were acquired in environments with lighting conditions that the network had trained on (all lights on or all off). The number of dynamic obstacles in the environments was negligible, so that ground-truth laser-based localization would not be affected. The camera’s view of the ceiling was not obstructed by people or other dynamic obstacles. This scenario was performed in environments A and B. The accuracy of the localization in this scenario demonstrates the viability of our approach.

Scenario 2 consisted in sampling the data from environment A while changing the artificial lighting conditions. During this scenario, we used lighting configurations where a subset of the lights was switched on. The training dataset for the CNNs did not contain this lighting configuration. While the accuracy of the localization is worse than with all lights on or off, our approach manages to produce a relatively stable localization. We also note that often, large spikes in pose error occur as the lights were switched on/off, probably due to the camera’s built-in brightness adaptation.

Table 1: Error of our approach relative to ground-truth.

Scenario and env.	Pose estimation error		
	Average and 95% confidence interval	Standard deviation	Max
<i>1A</i>	0.17±0.01m 0.13±0.02rad	0.12m 0.17rad	0.73m 1.60rad
<i>1B</i>	0.21±0.01m 0.10±0.01rad	0.14m 0.11rad	0.87m 1.18rad
<i>2A</i>	0.60±0.09m 0.32±0.05rad	0.87m 0.53rad	6.58m 3.03rad
<i>3B</i>	1.57±0.13m 0.26±0.02rad	1.57m 0.24rad	7.13m 2.20rad

Scenario 3 consisted in sampling the data from environment B while several people were present. People were instructed to walk or stand within 3m of the robot. This led to the robot’s view of the ceiling being partially obstructed by people’s faces and upper body. As a reminder, our network never trained on such conditions. Error for both position and orientation spiked when large parts of the ceiling were obstructed. Laser-based AMCL occasionally drifted, providing highly inaccurate pose estimations, an example of which is given in Fig. 8.

Orientation error behaved similarly to scenario 1, albeit with a slightly higher average error. Position error averaged above 3m for more than 30 consecutive samples three times, all in similar areas of the environment. To visualize which parts of the

image influenced the CNN output, we generated activation heatmaps for a high-error sample from scenario 3 and a low-error sample from a similar position in scenario 1 (see Fig. 9).

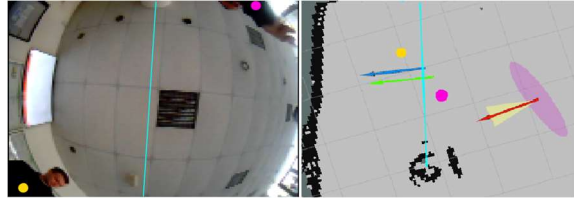


Figure 8: Left: camera image. Right: top-down view of the map (cells are 1m²). The vertical cyan line serves as a reference between the image and map. Arrows: actual robot position observed by the experimenter (green), our method (blue), laser-based amcl (red, with position and orientation uncertainties). Yellow and pink dots represent people.

We observe two differences between scenarios 1 and 3: (1) the combination of the pillar and lights in the top right corner of the image is a distinctive feature of this area, and it was blocked by a person in scenario 3. This could explain differences in activations seen in row 1 Fig. 9. (2) The lights in the corridor in the bottom left corner were always switched off during network training and in scenario 1, whereas they were on for scenario 3. This could explain the activation differences in rows 2 and 3 of Fig. 9. For orientation, the heatmaps were very similar except for the corridor area, which could explain the comparatively low error.

5 DISCUSSION

As with any supervised learning approach, we are highly dependent on the quality of the dataset. Acquiring ground truth data for the CNNs proved difficult, due to inaccuracies in the laser-based localization. There would be room for improvement if a more reliable ground truth method were used.

In order to deploy a robot using our method, one still needs to spend a fair amount of time acquiring the dataset and ensuring coverage of the whole environment, although this process could be automated with an environment exploration algorithm. Acquiring ground-truth supposes that one has access to an alternative method for localization, potentially requiring more expensive sensors. However, once the dataset has been acquired by a single robot, our method can be deployed on any number of robots using a simple inexpensive camera.

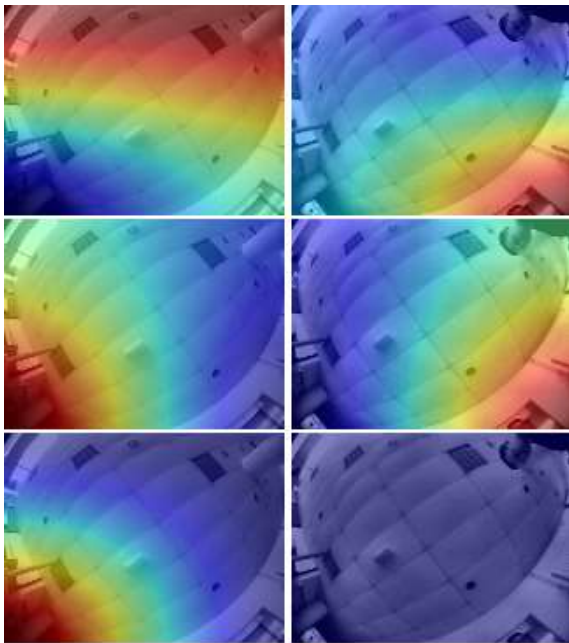


Figure 9: Comparison of position CNN output activation heatmaps generated using Keras-vis grad-cam (“keras-vis”), overlaid on the pre-processed image. Left to right: scenarios 1, 3. Top to bottom: heatmaps for areas that decrease, maintain, and increase the output values corresponding respectively to the “grad_modifier” parameters *negate*, *small_values*, and *None*. The “backprop_modifier” parameter was *None*.

Using the raw network predictions directly as the robot’s pose is currently unstable. The network occasionally outputs a pose with high error. This could be due to specific areas in the environment where the ceiling is too similar to another location. The accuracy loss when dealing with partial obstruction of the image by people could be reduced by mounting the camera higher on the robot, or potentially by using a fish-eye lens with less deformation. Further experiments would need to be conducted in truly crowded scenarios to confirm this.

Table 2 shows average position and orientation errors from recent 6-DoF camera relocalization works using the 7-scenes dataset where environments have an average size of 13 m³. While our work solves for the 3-DoF case, our test scenarios cover much larger environments, often with fewer distinctive features. Although the applications of our approach (3-DoF indoor robot localization) are different than the ones in the related works (6-DoF camera relocalization) we find it beneficial to provide such a comparison.

6 CONCLUSION

This work serves as an exploration into an original solution to global localization of a mobile robot in indoor environments. We have detailed a method to learn the correspondence between images of the ceiling and the robot’s position and orientation using a supervised learning approach (CNNs).

Our method was tested in two real environments with areas of around 72m² and 80m², with average position and orientation errors in the order of 0.19m and 0.11rad (median 0.16m, 0.07rad) in uncrowded environments. These results indicate that our method has some potential, especially considering the modest hardware requirements in terms of sensors and processing power. Tests were performed with varied artificial lighting conditions where our method showed some degree of robustness to lighting changes. Partial obstruction of the ceiling images by people standing near the robot led to significantly higher errors in position estimation, and a relatively small increase in orientation estimation errors.

Table 2: Comparison to 6-DoF camera relocalization work

Approach	Dataset	Median position error	Median orientation error
VIDLOC (Clark et al., 2017)	7-scenes	0.26m	N/A
PoseNet(Kendall et al, 2015)	7-scenes	0.48m	0.17rad
MapNET (Brahmbhatt et al., 2018)	7-scenes	0.20m	0.11rad
MapNET PGO(Brahmbhatt et al., 2018)	7-scenes	0.18m	0.11rad
Ours	Scenario 1	0.16m	0.07rad

7 FUTURE WORK

In order to better deal with crowded environments, a training dataset could be acquired when people are present in the environment. Such a dataset would potentially be harder to acquire; however, the network should be able to provide better localization than when trained on a dataset of a static environment. The existing dataset could be modified by adding people at random locations in the images.

In order to incorporate this work into a complete localization framework, we can filter the output of the

pose prediction networks to provide a more stable estimate. One could also consider a set of poses over time in order to discard outliers. The stable pose estimation can be combined with other localization data such as odometry using sensor fusion.

The speed of the pose update could be improved by adopting a more elaborate CNN architecture. Recent CNN architectures can minimize resource usage while maintaining good accuracy for their tasks (Zhang et al., 2018). Further experimentation with architectures and hyper parameters could also improve accuracy and inference time.

ACKNOWLEDGEMENTS

This work has been partially supported by MIAI @ Grenoble Alpes, (ANR-19-P3IA-0003).

REFERENCES

- Brahmbhatt, S., Gu, J., Kim, K., Hays, J., & Kautz, J. (2018). Geometry-aware Learning of Maps for camera localization. *2018 IEEE/CVF Conference on Computer Vision and Pattern Recognition*, 2616–2625.
- Burgard, W., Cremers, A. B., Fox, D., Hähnel, D., Thrun, S., Dellaert, F., Bennewitz, M., Rosenberg, C., Roy, N., Schulte, J., & Schulz, D. (1999). MINERVA: A second generation mobile tour-guide robot. *Proceedings of the IEEE International Conference on Robotics and Automation (ICRA)*.
- Clark, R., Wang, S., Markham, A., Trigoni, N., & Wen, H. (2017). Vidloc: A deep spatio-temporal model for 6-dof video-clip relocalization. *2017 IEEE Conference on Computer Vision and Pattern Recognition (CVPR)*, 2652–2660.
- Delibasis, K. K., Plagianakos, V. P., & Maglogiannis, I. (2015). Estimation of robot position and orientation using a stationary fisheye camera. *International Journal on Artificial Intelligence Tools*, 24(06), 1560004.
- Dellaert, F., Fox, D., Burgard, W., & Thrun, S. (1999). Monte Carlo localization for mobile robots. *Proceedings 1999 IEEE International Conference on Robotics and Automation (Cat. No.99CH36288C)*, 2, 1322–1328.
- Durrant-Whyte, H., & Bailey, T. (2006). Simultaneous localization and mapping: Part I. *IEEE Robotics & Automation Magazine*, 13(2), 99–110.
- Ioffe, S., & Szegedy, C. (2015). Batch Normalization: Accelerating Deep Network Training by Reducing Internal Covariate Shift. *Proceedings of the 32nd International Conference on Machine Learning*.
- Jeong, W., & LEE, K. M. (2005). CV-SLAM: a new ceiling vision-based SLAM technique. *2005 IEEE/RSJ International Conference on Intelligent Robots and Systems*.
- Jin, T., & Lee, J. (2004). Mobile robot navigation by image classification using a neural network. *IFAC Proceedings Volumes*, 37(12), 203–208.
- Kendall, A., & Cipolla, R. (2017). Geometric loss functions for camera pose regression with deep learning. *2017 IEEE Conference on Computer Vision and Pattern Recognition (CVPR)*, 6555–6564.
- Kendall, A., & Cipolla, R. (2016). Modelling uncertainty in deep learning for camera relocalization. *2016 IEEE International Conference on Robotics and Automation (ICRA)*, 4762–4769.
- Kendall, A., Grimes, M., & Cipolla, R. (2015). Posenet: A convolutional network for real-time 6-dof camera relocalization. *2015 IEEE International Conference on Computer Vision (ICCV)*, 2938–2946.
- King, S. J., & Weiman, C. F. R. (1991). *HelpMate autonomous mobile robot navigation system* (W. H. Chun & W. J. Wolfe, Eds.; pp. 190–198).
- Kotikalapudi, R. A. C. (n.d.). *Keras-vis*. <https://github.com/raghakot/keras-vis>
- Krizhevsky, A., Sutskever, I., & Hinton, G. E. (2012). ImageNet classification with deep convolutional neural networks. *Proceedings of the 25th International Conference on Neural Information Processing Systems*.
- Nourbakhsh, I. (1998). *The failures of a self-reliant tour robot with no planner*.
- Pizer, S. M., Amburn, E. P., Austin, J. D., Cromartie, R., Geselowitz, A., Greer, T., ter Haar Romeny, B., Zimmerman, J. B., & Zuiderveld, K. (1987). Adaptive histogram equalization and its variations. *Computer Vision, Graphics, and Image Processing*, 39(3), 355–368.
- Reddi, S. J., Kale, S., & Kumar, S. (2018). *On the Convergence of Adam and Beyond*. International Conference on Learning Representations.
- RobAIR. (n.d.). LIG FabMSTIC. <https://air.imag.fr/index.php/RobAIR>
- Szegedy, C., Wei Liu, Yangqing Jia, Sermanet, P., Reed, S., Anguelov, D., Erhan, D., Vanhoucke, V., & Rabinovich, A. (2015). Going deeper with convolutions. *2015 IEEE Conference on Computer Vision and Pattern Recognition (CVPR)*, 1–9.
- Thrun, S. (1998). Finding landmarks for mobile robot navigation. *Proceedings. 1998 IEEE International Conference on Robotics and Automation (Cat. No.98CH36146)*, 2, 958–963.
- Xiao, L., Wang, J., Qiu, X., Rong, Z., Zou, X. (2019) Dynamic-SLAM: Semantic monocular visual localization and mapping based on deep learning in dynamic environment. *Robot. Auton. Syst.*, 117, 1–16.
- Zhang, F., Duarte, F., Ma, R., Miliotis, H., Lin, H., & Ratti, C. (2016). Indoor Space Recognition using Deep Convolutional Neural Network: A Case Study at MIT Campus. *PLoS ONE*.
- Zhang, X., Zhou, X., Lin, M., & Sun, J. (2018). Shufflenet: An extremely efficient convolutional neural network for mobile devices. *2018 IEEE/CVF Conference on Computer Vision and Pattern Recognition*, 6848–6856.